Available online at www.sciencedirect.com
ScienceDirect
Astroparticle Physics 27 (2007) 512–520
Astroparticle Physics
www.elsevier.com/locate/astropart

Search for point-like sources of cosmic rays with energies above $10^{18.5}$ eV in the HiRes-I monocular data set

The High-Resolution Fly's Eye Collaboration

R.U. Abbasi [a], T. Abu-Zayyad [a], J.F. Amann [b], G. Archbold [a], K. Belov [a], J.W. Belz [a], S. BenZvi [c], D.R. Bergman [d], S.A. Blake [a], Z. Cao [a], B.M. Connolly [c], W. Deng [a], Y. Fedorova [a], J. Findlay [a], C.B. Finley [c], R.C. Gray [a], W.F. Hanlon [a], C.M. Hoffman [b], M.H. Holzscheiter [b], G.A. Hughes [d], P. Hüntemeyer [b], B.F. Jones [a], C.C.H. Jui [a], K. Kim [a], M.A. Kirn [e,*], E.C. Loh [a], M.M. Maestas [a], N. Manago [f], L.J. Marek [b], K. Martens [a], J.A.J. Matthews [g], J.N. Matthews [a], S.A. Moore [a], A. O'Neill [c], C.A. Painter [b], L. Perera [d], K. Reil [a], R. Riehle [a], D. Rodriguez [a], M.D. Roberts [g], M. Sasaki [f], S.R. Schnetzer [d], L.M. Scott [d], G. Sinnis [b], J.D. Smith [a], P. Sokolsky [a], C. Song [c], R.W. Springer [a], B.T. Stokes [a], J.R. Thomas [a], S.B. Thomas [a], G.B. Thomson [d], D. Tupa [b], S. Westerhoff [c], L.R. Wiencke [a], A. Zech [d], X. Zhang [c]

[a] *University of Utah, Department of Physics and High Energy Astrophysics Institute, Salt Lake City, UT, USA*
[b] *Los Alamos National Laboratory, Los Alamos, NM, USA*
[c] *Columbia University, Department of Physics and Nevis Laboratory, New York, NY, USA*
[d] *Rutgers – The State University of New Jersey, Department of Physics and Astronomy, Piscataway, NJ, USA*
[e] *Montana State University, Department of Physics, Bozeman, MT, USA*
[f] *University of Tokyo, Institute for Cosmic Ray Research, Kashiwa, Japan*
[g] *University of New Mexico, Department of Physics and Astronomy, Albuquerque, NM, USA*

Received 24 May 2005; received in revised form 14 February 2007; accepted 15 March 2007
Available online 24 March 2007

Abstract

We report the results of a search for point-like deviations from isotropy in the arrival directions of ultra-high energy cosmic rays in the northern hemisphere. In the monocular data set collected by the High-Resolution Fly's Eye, consisting of 1525 events with energy exceeding $10^{18.5}$ eV, we find no evidence for point-like excesses. We place a 90% c.l. upper limit of 0.8 hadronic cosmic rays/km^2 yr on the flux from such sources for the northern hemisphere and place tighter limits as a function of position in the sky.
Published by Elsevier B.V.

Keywords: Cosmic rays; Anisotropy; Point source; HiRes

1. Introduction

In the search for compact sources of ultra-high energy cosmic rays (UHECR), a variety of strategies have been employed, yielding ambiguous results. Excesses have been

* Corresponding author. Tel.: +1 301 963 5161.
E-mail address: kirn@fnal.gov (M.A. Kirn).

0927-6505/$ - see front matter Published by Elsevier B.V.
doi:10.1016/j.astropartphys.2007.03.002

reported in the vicinity of the galactic center [1,2], and alternately claimed and refuted in the vicinity of Cygnus X-3 [3–6], an X-ray binary within our galaxy, including the report of a possible excess in a point-like source search [7]. The HiRes [8–10] and Akeno Giant AirShower Array (AGASA) [11–14] experiments disagree on the existence of point-like clusters of particles with energies above 4×10^{19} eV. Recently, possible correlations between UHECR arrival directions and BL-Lacertae (BL Lac) objects have been the subject of study. The earliest reported correlations between events observed by AGASA and Yakutsk [15,16] with subsets of BL Lacs from the Véron catalog and Véron [17] have not been confirmed with HiRes stereo data [18]. However, correlations have been observed between HiRes stereo data above 10 EeV and BL Lac objects, with chance probabilities at the 10^{-3} level [18,19].

In addition to the observational ambiguities, there are theoretical difficulties in understanding point-like sources with energies at or below 10 EeV. Both galactic and extragalactic magnetic fields are expected to produce large perturbations in the arrival directions of charged particles: a proton with an energy of a few EeV may be deflected by several degrees – more than the angular resolution of contemporary airshower detectors – as it traverses the disk of the Milky Way galaxy, with a typical magnetic field of order 1 microgauss [20]. At higher energies, models have been proposed in which arrival direction clustering of charged primaries is permitted by regions of anomalously small galactic magnetic fields [21,22]. However, these scenarios seem particularly unlikely at energies as low as $10^{18.5}$ eV.

A compact arrival direction excess at these energies therefore appears to require neutral primaries. Neutrons possess a lifetime of 3×10^{12} s at 10 EeV and so cannot have originated more than 100 kpc from Earth. The mean-free path of photons at these energies is of order a few Mpc. Thus any viable source of standard model neutral matter would have to be located within or nearby the Milky Way Galaxy. This requirement allows models in which neutrons are emitted from the galactic center [23–28], but contradicts the BL Lac hypothesis.

While models have focused on the galactic center as a likely source of neutron flux, the point-like excess observed in the SUGAR data [2] was located 7.5° from the galactic center. This indicates the possibility of an accidental line-of-sight alignment and motivates the search for point-like sources elsewhere in the sky, including that portion viewed from the northern hemisphere.

In this paper, we conduct a study complementary to previous searches for point-like (within detector resolution) arrival direction excesses for cosmic ray events above $10^{18.5}$ eV in the northern hemisphere. We use a skymap technique in which we evaluate our sensitivity using Monte Carlo simulated sources and place upper limits on the flux of hadrons from point-like sources, including the historically significant source candidate Cygnus X-3.

2. The HiRes-I monocular data set

The High-Resolution Fly's Eye (HiRes) consists of two nitrogen fluorescence observatories – HiRes-I and HiRes-II – separated by 12.6 km and located at Dugway, Utah [29–31]. HiRes-I is located at 40.195°N. latitude and 112.836°W. longitude, at an altitude of 1597 m above mean sea level. HiRes was conceived as a stereo detector, however, due to the larger available statistics it is desirable to reconstruct extensive airshowers in monocular mode as well. The HiRes-I monocular data set used in this analysis consists of 2820 good-weather detector hours of data, collected between May 1997 and February 2003.

The HiRes-I monocular data set and airshower reconstruction by the profile-constrained fitting technique has recently been described in the literature [32]. The shower selection criteria for the present data set can be summarized as follows [29,32,33]:

- A minimum of three good photomultiplier tubes (PMTs) are used in reconstructing the event. Each PMT subtends approximately $1° \times 1°$.
- The observed airshower length must be greater than 7.9°.
- The measured angular speed of the airshower must be less than 3.33°/μs.
- The average number of photons per PMT must be greater than 200.
- The calculated Cherenkov-light contribution to the observed signal must not exceed 20% for more than two PMTs.
- The depth of the first observed point of the airshower must be less than 1000 g/cm^2.
- The angle of the track within the shower-detector plane (Ψ in Fig. 1) must be less than 120° to limit Cherenkov-light contamination to the fluorescence signal.

After the above cuts, a total of 1525 airshower events with energies exceeding $10^{18.5}$ eV were collected and are included in the present analysis. Note that the above cuts, tuned for hadron-induced showers, render HiRes insensitive to gamma-induced showers. Therefore, in the present work, we do not attempt to place limits on gamma ray sources.

A residual effect of the profile-constrained fitting technique is orientation-dependent (elliptical) uncertainties in the airshower arrival directions. In Fig. 1, the airshower reconstruction geometry is illustrated for a monocular air fluorescence detector. In this view, the shower-detector plane (SDP) for HiRes-I events is well-reconstructed, with uncertainty parameterized as

$$\sigma_{\mathrm{SDP}} = 88.2° e^{-\Delta\chi/1.9595} + 0.37° \quad (1)$$

where $\Delta\chi$ is the angular tracklength of the shower in degrees. Typical values of σ_{SDP} for this analysis range from 0.4° to 1.7°. The angle of the track within the SDP, Ψ, is less well reconstructed and is parameterized by

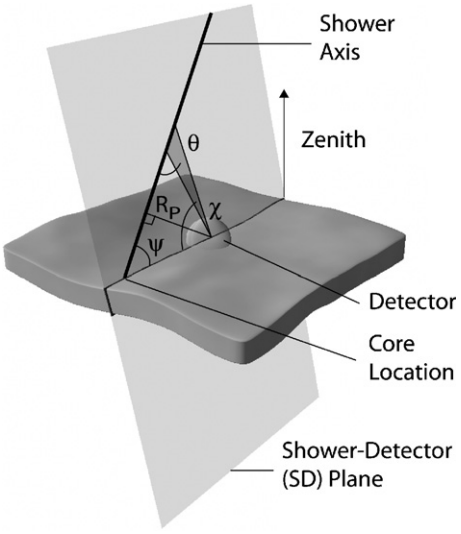

Fig. 1. The geometry of reconstruction for monocular air fluorescence detector. R_P is the shower's distance of closest approach, Ψ is the angle of the shower within the shower-detector plane (uncertainty parametrized in Eq. (2)), and χ is the angular tracklength of the shower.

$$\sigma_\Psi = 18.4^\circ e^{-\log_{10}(E)/0.69085} + 4.1^\circ \quad (2)$$

where the energy E is expressed in EeV (10^{18} eV). Typical values of σ_Ψ in this analysis range from 5.4° to 15°. The parameterizations of Eqs. (1) and (2) are carried out in Ref. [34].

In Fig. 2, we plot the skymap formed from the arrival directions of events in the present data set. Each event's "error ellipse" is represented by generating 1000 points per event, distributed according to the Gaussian error model of Eqs. (1) and (2). Fig. 2 is plotted in equatorial coordinates as a polar plot. Note that bins are assigned using a cartesian projection of the polar plot shown in Fig. 2 and all similar figures. As such,angular bin size varies across the map, but averages approximately $1^\circ \times 1^\circ$.

We next discuss the Monte Carlo technique, by which we evaluate the significance of fluctuations in the skymap as well as our sensitivity to point-like behavior in arrival direction.

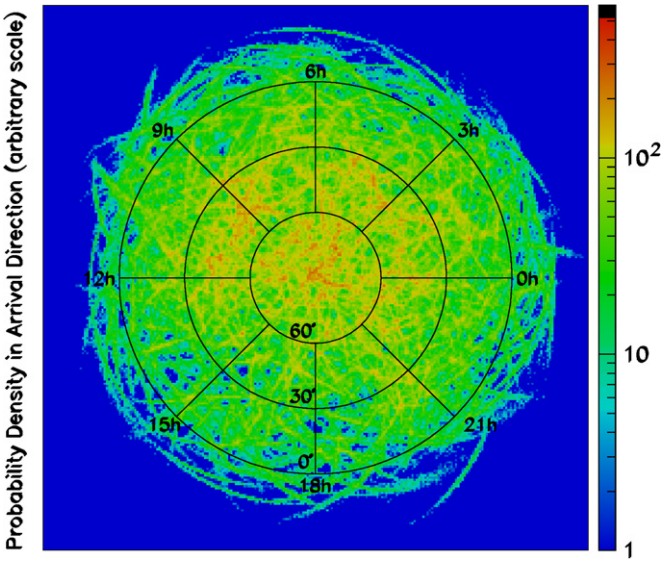

Fig. 2. Skymap of arrival directions of events in the HiRes-I monocular data set, plotted in polar projection, equatorial coordinates. Each HiRes event is represented by 1000 points randomly thrown according to the elliptical Gaussian error model of Eqs. (1) and (2). The z (color) axis of this plot is logarithmic and arbitrary. The bin size in this plot (and all similar plots) is approximately $1^\circ \times 1^\circ$.

3. The Monte Carlo; comparison of data to expectation from an isotropic background

We use a library of simulated events, generated by the Monte Carlo technique and reconstructed using the profile-constrained reconstruction program to determine the background expectation for isotropically distributed sources as well as to evaluate our sensitivity to point-like behavior in arrival direction. For this library, we assume an isotropic distribution for events possessing the spectrum and composition suggested by the stereo Fly's Eye experiment [35,36]: spectral indices of −2.6 for protons and −3.5 for iron with an equal differential flux at $10^{18.4}$ eV. As of this writing, the Fly's eye stereo result is the only independent combined spectrum and composition measurement in this energy range.

A detector runtime database is used to randomly assign a time from detector "on" periods to each event in the isotropic background data set. A total of 1000 isotropic data sets with the same sky exposure as the HiRes-I monocular data set were generated for comparison studies. Further discussion of this Monte Carlo can be found in Ref. [37]. In Figs. 3 and 4, we compare the data and Monte Carlo distributions of events in the variables right ascension (RA) and declination (DEC), respectively.

In order to understand the significance of the fluctuations in Fig. 2, we compare the data on a bin-by-bin basis to the 1000 simulated data sets. Defining N_{DATA} as the bin density of the data, N_{MC} as the bin density of the simulated

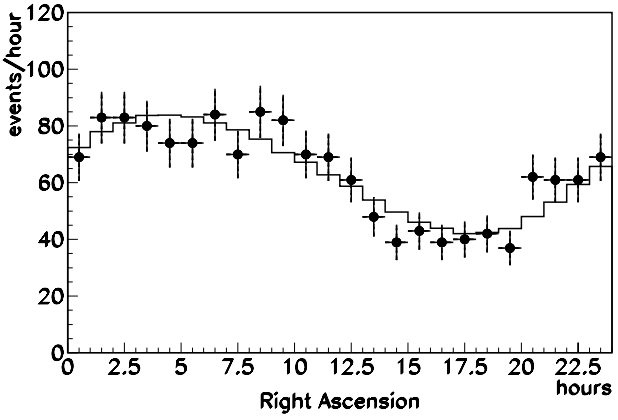

Fig. 3. Comparison of HiRes-I data (points) and Monte Carlo (solid histogram) distributions in right ascension (RA).

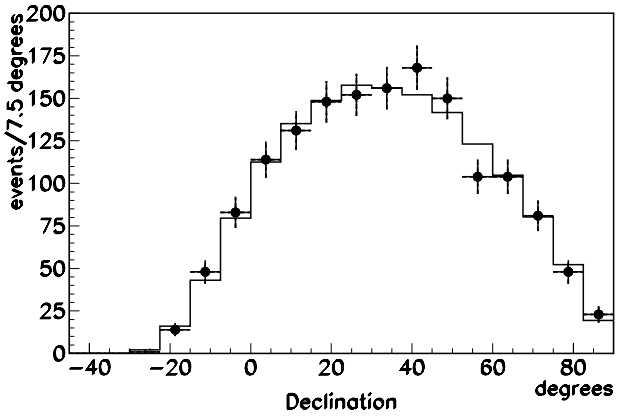

Fig. 4. Comparison of HiRes-I data (points) and Monte Carlo (solid histogram) distributions in declination (DEC).

isotropic data sets, and σ_{MC} as the standard deviation of the Monte Carlo bin density, the variable

$$\xi = \frac{N_{DATA} - \langle N_{MC} \rangle}{\sigma_{MC}} \quad (3)$$

provides a measure of the fluctuation per bin. Fig. 5 shows the distribution of ξ as a function of position in the sky for the HiRes-I monocular data set.

The distribution of ξ is non-Gaussian (Fig. 6). Thus, it is necessary to develop a technique to evaluate the significance of possible sources. Our technique uses the ξ information in neighboring bins to pick out significant fluctuations above background from the skymap. The parameters in the technique are tuned on simulated point-like sources.

4. The Monte Carlo; simulation of point-like sources

We have two objectives in simulating point-like sources: the first is using the simulated sources to tune point excess

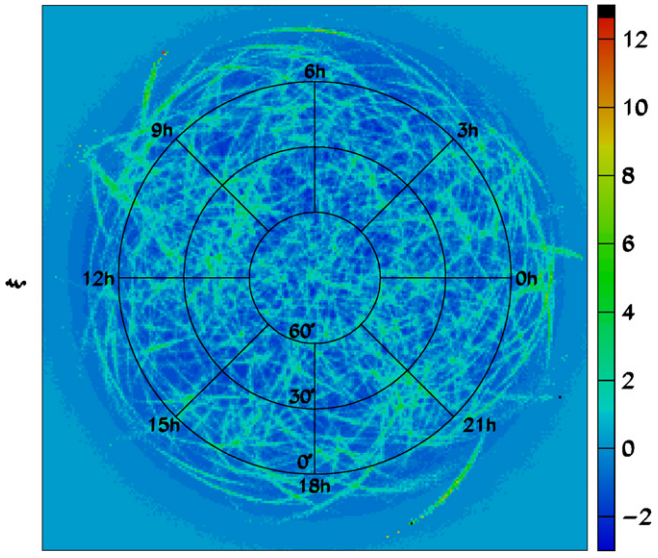

Fig. 5. ξ (Eq. (3)) distribution for the HiRes-I monocular data set.

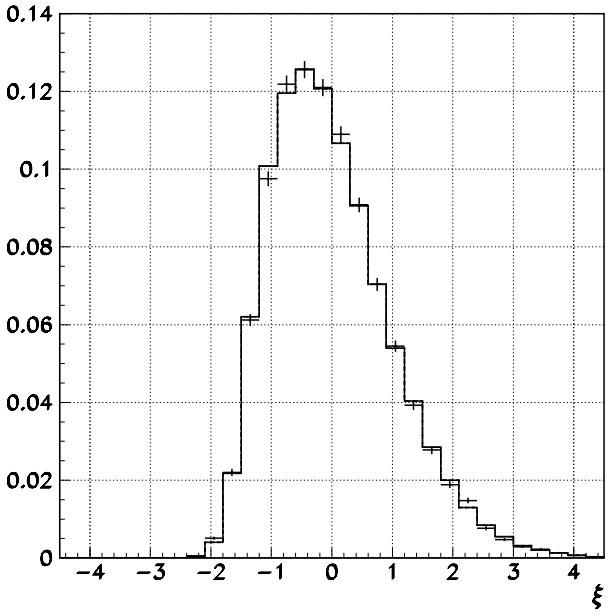

Fig. 6. Distribution in ξ of data (points) and Monte Carlo (histogram) for all bins with DEC greater than 0°. Both distributions are normalized to have unit area.

selection criteria. Secondly, simulated sources provide a straightforward method by which to quantify our sensitivity to point-like excesses and derive flux upper limits.

Simulated source skymaps are created by randomly replacing events in a simulated isotropic data set with N_S events at the chosen position for the source. The energy and error ellipse are taken from the replaced event and the ellipse orientation is randomized. Finally, the central-value coordinates of the simulated source event are randomly shifted according to the error ellipse, simulating the effect of detector resolution.

In choosing this technique, we implicitly assume our sources have the same spectrum and hadronic composition as the isotropic background. However, as discussed in Section 1, many models predicting point-like excesses point to neutrons as the primary cosmic ray. The differences between neutron sources and sources consisting of a proton–iron mix are small in this case. The HiRes-I detector aperture above $10^{18.5}$ eV is approximately 15% greater for nucleon-induced showers than for the proton–iron mix [29]. This is due to poor reconstruction of iron showers which tend to shower earlier in the atmosphere than protons. This effect results in our stating slightly more conservative upper limits then we would have had we used neutrons exclusively in our point source simulations. Secondly, the error ellipses for iron nuclei differ in length from those associated with protons and neutrons by about 5%. This contributes a small amount to our systematic uncertainty in the number of source events, N_S, as discussed in Section 6.1.

An example of a simulated source is shown in Fig. 7. This source is superimposed on a Monte Carlo data set in Fig. 8, and the quantity ξ (Eq. (3)) is evaluated for each

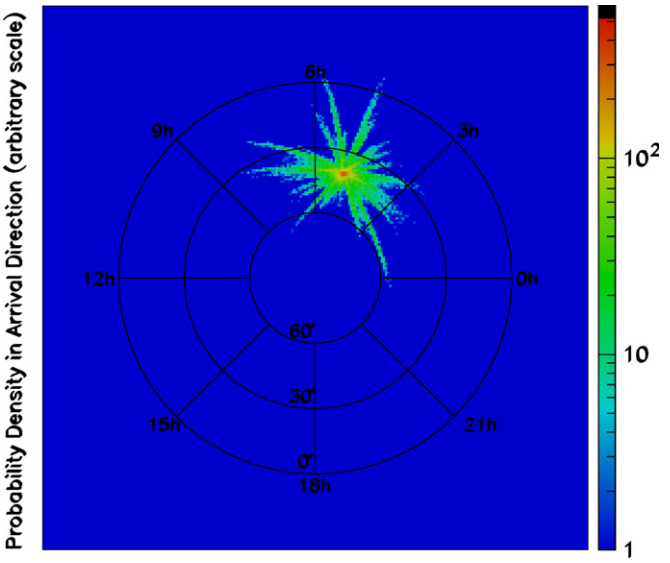

Fig. 7. An $N_S = 25$ event source shown without the isotropic background. The source has been inserted at 5 h RA, 40° DEC. Each source event is represented by 1000 points randomly thrown according to the elliptical Gaussian error model of Eqs. (1) and (2), where the error ellipse is taken from the replaced isotropic event. Twelve percentage of points on this graph lie within a circle of 2.5° radius centered on the source coordinates. Sixty-eight percentage of points are contained within a circle of 13° radius centered on the source coordinates.

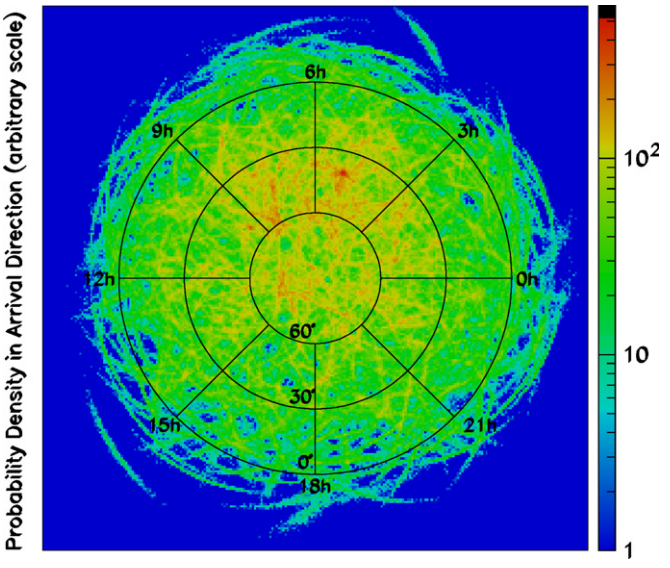

Fig. 8. Skymap of arrival directions of events for a simulated data set, having the same overall exposure as the HiRes-I monocular data set, with a 25 event source superimposed at 5 h RA, 40° DEC (compare to Fig. 2).

bin in Fig. 9. We note that source events overlap in a fairly small angular region, as seen in Fig. 7. Thus, we have sensitivity to fairly compact deviations from isotropy, despite our elongated error ellipses.

5. Calculation of significances

We now describe a procedure by which we can identify point-like behavior in arrival direction (for example,

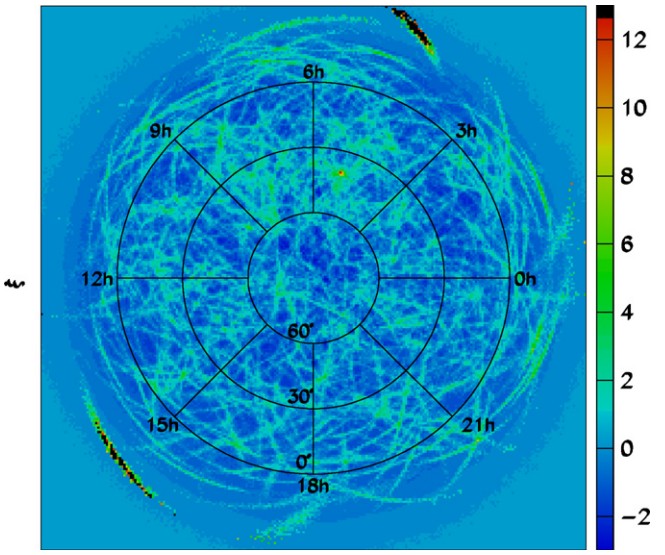

Fig. 9. ξ (Eq. (3)) for $N_S = 25$ event source inserted in an simulated isotropic data set. The source has been inserted at 5 h RA, 40° DEC (compare to Fig. 5).

the simulated source of Figs. 7–9) while simultaneously rejecting false positives arising from fluctuations of the background.

Due to detector resolution, it is desirable that we search for sources by considering points over an extended angular region. We consider a "search circle" of radius R, where R is expressed as an angle in degrees. Within the search circle, we count the fraction of bins F having an ξ value greater than some threshold ξ_{THR}. The parameters R and ξ_{THR} are chosen to optimize the signal size, and a cut is chosen on the fraction F which reduces the false positive probability to an acceptable level.

Our maximum sensitivity to point-like behavior in arrival direction, given the HiRes-I pointing uncertainty, was determined to require a search circle of $R = 2.5°$, and a value $\xi_{THR} = 4$. (In the case in which the bin densities are normally distributed, this corresponds to 4σ.) The optimum values for these parameters were determined by simulating sources at various locations in the sky and maximizing our sensitivity to these sources. The values for these parameters are found to be largely insensitive to the position in the sky and the number of events in the source. Additionally, small variations in either of these parameters do not have a significant impact on our results.

Due to low statistics at the edge of HiRes' acceptance, we consider only search circles with centers whose declinations are greater than 0°. That is, we only search for sources north of the celestial equator. Approximately 10% of HiRes events have central-value coordinates south of the equator. These events can contribute to the search if their error ellipses extend north of DEC = −2.5°.

In Fig. 10, we have plotted for each bin the fraction F, for $R = 2.5°$ and $\xi_{THR} = 4$, of the simulated point source of Fig. 8. The simulated source stands out clearly in this figure.

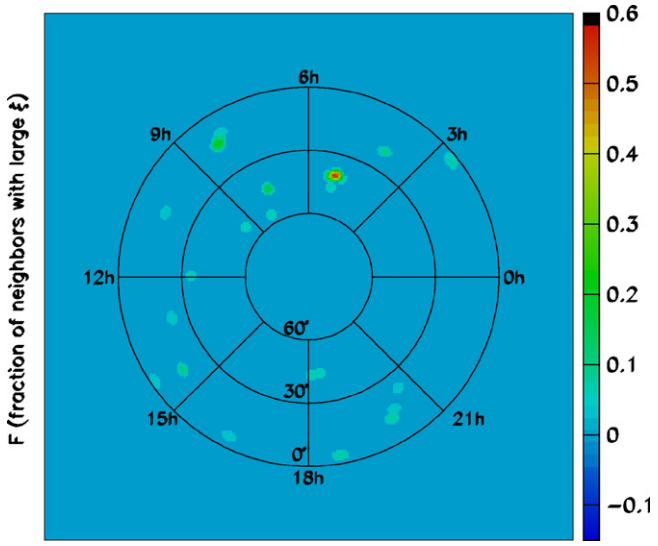

Fig. 10. F distribution derived from the ξ map of Fig. 9. F is the fraction of bins within radius $R = 2.5°$ having a ξ value of 4 or greater. The simulated source at 5 h RA, 40° DEC clearly stands out as having an exceptionally large excess fraction F.

The final parameter in this search algorithm is the cut placed on the quantity F. We evaluate this cut by requiring that the probability of a simulated isotropic data set – *without* a superimposed simulated source – exceeding the cut be no more than 10% over the entire sky (Fig. 11). We choose a cut value of $F = 0.33$, corresponding to a false-positive probability of 10%.

Fig. 12 shows the F distribution for the monocular data set. The "hottest" spot on this graph, near DEC = 20° and RA = 20 h, has a value $F = 0.15$. 87% of simulated isotropic data sets have a maximum value of $F \geqslant 0.15$ (see

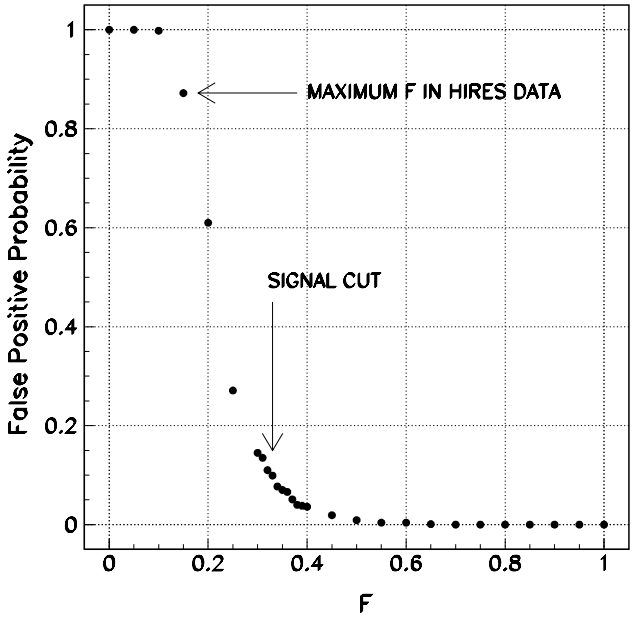

Fig. 11. Occurrence rate of false positives versus F, for a 2.5° search circle and ξ threshold of 4. A cut at $F = 0.33$ corresponds to a false-positive probability of 10%.

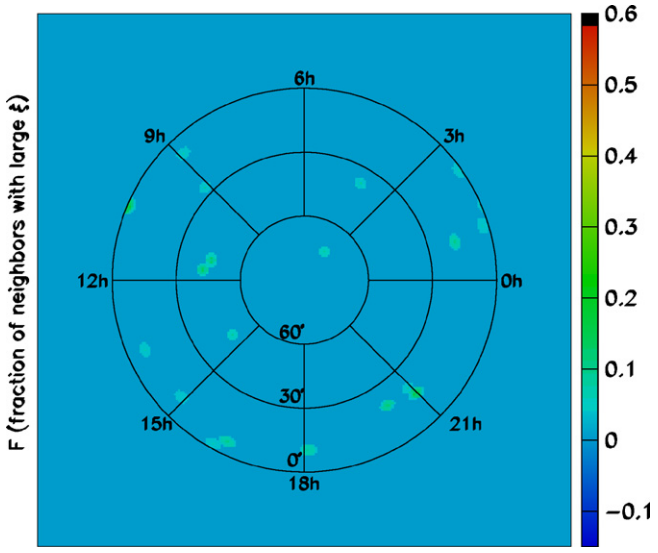

Fig. 12. F distribution derived from the HiRes-I monocular data (Figs. 2 and 5). F is the fraction of bins within radius $R = 2.5°$ having a ξ value of 4 or greater. No points satisfy our search criteria. The largest F occurs at DEC = 20° and RA = 20 h and has a value $F = 0.15$, corresponding to a false-positive probability of 87%.

Fig. 11). We conclude that our observation is consistent with a fluctuation from an isotropic background.

Next, we evaluate the corresponding sensitivity and flux upper limits as a function of position in the sky.

6. Sensitivity and upper limits

In Section 5, we found no evidence for the presence of point-like excesses in the HiRes-I monocular data set above $10^{18.5}$ eV. Further, the significance of the largest point-like fluctuation in the data is well below the threshold established to minimize the likelihood of false positives in an isotropic distribution. To quantify our null result, we follow the suggestion of Feldman and Cousins [38] and calculate both a set of flux upper limits and the "sensitivity" of the experiment to such point-like excesses. The results of these calculations are reported below.

6.1. Sensitivity

The sensitivity of the experiment is defined as the average 90% confidence level flux upper limit that would be reported by an ensemble of like experiments with no true signal. Since this will vary as a function of position on the sky due to different background expectations, we calculate our sensitivity at a set of gridpoints (Table 1) distributed evenly across the Northern Hemisphere. We choose the right ascension values of our gridpoints to correspond approximately to the HiRes "solstices" and "equinoxes", i.e., to the RA lines of high, low and midrange event statistics.

To determine our sensitivity to a number of "source" events $\langle N_S \rangle$ at a given gridpoint, we generate 400 simulated

Table 1
Locations of gridpoints, threshold signal strengths $N_{.33}$ and $N_{.15}$, mean number of Monte Carlo events, exposures (with uncertainty 5%, primarily from Monte Carlo statistics), detector flux sensitivity, and 90% confidence level flux upper limits, for cosmic rays with energy exceeding $10^{18.5}$ eV

DEC (degr)	RA (h)	$N_{.33}$	$N_{.15}$	$\langle N_{MC}\rangle$ in 2.5°	Exposure (km^2 yr)	Sensitivity (km^{-2} yr^{-1})	Upper limit (km^{-2} yr^{-1})
15°	2.5	23	16	1.3	34.2	.7	.5
	5.5	24	19	1.4	36.6	.7	.5
	8.5	22	16	1.2	34.3	.6	.5
	11.5	20	16	1.1	24.5	.8	.7
	14.5	18	14	.8	21.9	.8	.6
	17.5	18	13	.7	16.7	1.1	.8
	20.5	17	13	.7	21.1	.8	.6
	23.5	21	16	1.2	26.7	.8	.6
45°	2.5	26	20	1.8	49.7	.5	.4
	5.5	29	22	2.0	56.6	.5	.4
	8.5	25	20	1.7	48.5	.5	.4
	11.5	24	18	1.5	41.2	.6	.4
	14.5	21	15	1.2	33.5	.6	.4
	17.5	21	16	1.0	24.9	.8	.6
	20.5	21	16	1.2	30.3	.7	.5
	23.5	24	18	1.5	41.5	.6	.4
75°	5.5	29	21	2.2	59.8	.5	.4
	11.5	28	21	2.1	50.5	.6	.4
	17.5	26	19	1.8	38.6	.7	.5
	23.5	26	20	2.0	47.2	.6	.4
90°	N/A	31	23	2.5	53.8	.6	.4

isotropic datasets with $\langle N_S\rangle$ isotropic events replaced by point-like source events. The number of events in each source is Poisson distributed with mean value $\langle N_S\rangle$. These datasets contain the same total number of events as the HiRes-I data.

We then determine the percentage of trials at each location for which our reconstruction algorithm "finds" a source of size $\langle N_S\rangle$. In the case of the sensitivity calculation, we say the algorithm "finds" a source if at one point on the skymap F fluctuates above our preselected threshold value of $F = 0.33$. The value of $\langle N_S\rangle$ for which signal was declared for 90% or better of the trials was termed $N_{.33}$.

The distribution of $N_{.33}$ at our grid points is illustrated in Fig. 13. The chief source of systematic uncertainty in the calculation of $N_{.33}$ is uncertainties in the size of the error ellipses. To allow for the difference in error ellipses for iron and neutron/proton induced showers (as discussed in Section 4) as well as additional reconstruction uncertainties at the 5% level, we conducted a study in which we decreased the size of the error ellipses by 20% and found that at our gridpoints the effect on $N_{.33}$ was $\leqslant 1$ event. We thus assign a systematic uncertainty of ± 1 event to $N_{.33}$.

The HiRes-I detector flux sensitivity at each grid point is $N_{.33}$ at that point divided by the local exposure. We calculate the detector exposure [34] for point sources at the grid points by the following procedure: Monte Carlo events are generated at the grid points, assigned a time from the distribution of HiRes detector ontimes, and projected towards the detector aperture. Local coordinates and times are determined, then the event is paired with a shower from the Monte Carlo event library having similar local coordinates. An attempt is then made to reconstruct the Monte Carlo event with the profile-constrained fitting technique. The exposure, defined as the fraction of events reconstructed multiplied by the detector aperture (area) and time, can then be used to determine flux sensitivity (as well as flux upper limits) for each of the grid locations. These exposures are listed in Table 1. The final flux sensitivities are shown in Table 1 and Fig. 14.

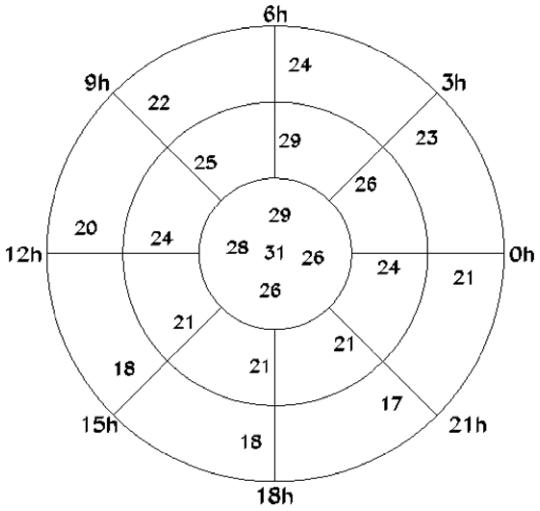

Fig. 13. Numerical values of $N_{.33}$ – the mean number of source events for which signal was declared in 90% or better of 400 trials with a cut on F of .33 – at 21 grid points in the Northern Hemisphere. Exact numbers and locations of gridpoints are given in Table 1. The systematic uncertainty in the calculation of $N_{.33}$, due to uncertainties in the size of the error ellipses, is $\leqslant 1$ event.

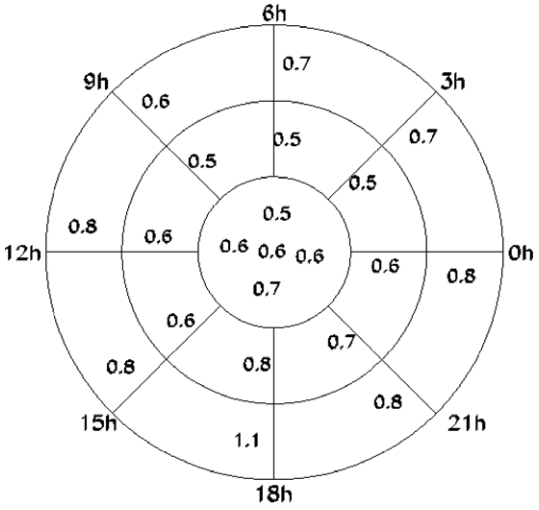

Fig. 14. Flux sensitivity ($km^{-2}\,yr^{-1}$) at 21 grid points in the Northern Hemisphere. Sensitivity is calculated by dividing $N_{.33}$ (Fig. 13) by the exposure at each grid point. The numbers along with the exact locations of grid points are given in Table 1.

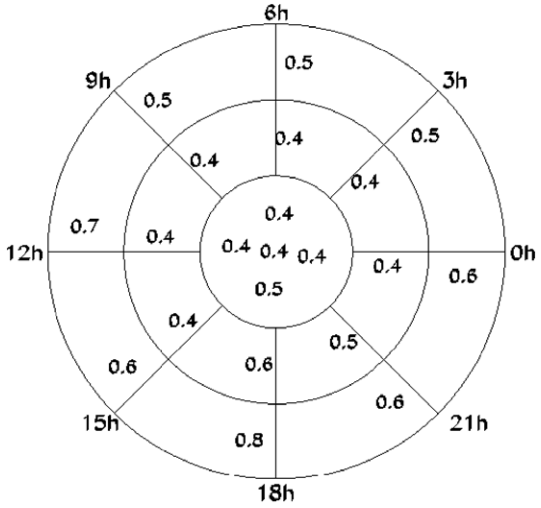

Fig. 16. Ninety percent c.l. flux upper limit ($km^{-2}\,yr^{-1}$) at 21 grid points in the Northern Hemisphere. Flux upper limit is calculated by dividing $N_{.15}$ by the exposure at each grid point. Exact numbers and locations of gridpoints are given in Table 1.

6.2. Upper limits

We place our 90% confidence level flux upper limits by making use of the fact that F never fluctuated above 0.15 in the HiRes-I data (Fig. 10). We determine the value of $N_{.15}$ – the mean number of source events for which signal was declared in 90% or better of trials with a threshold of $F = .15$ – in the same manner in which we determined $N_{.33}$ in Section 6. The results are summarized in Fig. 15. Our 90% c.l. flux upper limit at each grid point (Fig. 16) is $N_{.15}$ at that point divided by the local exposure. The largest flux upper limit is 0.8 hadronic cosmic rays above $10^{18.5}$ eV per km^2 yr.

Note that the flux sensitivities and upper limits can be readily extrapolated for points not on the grid, because the values vary smoothly as a function of position on the sky.

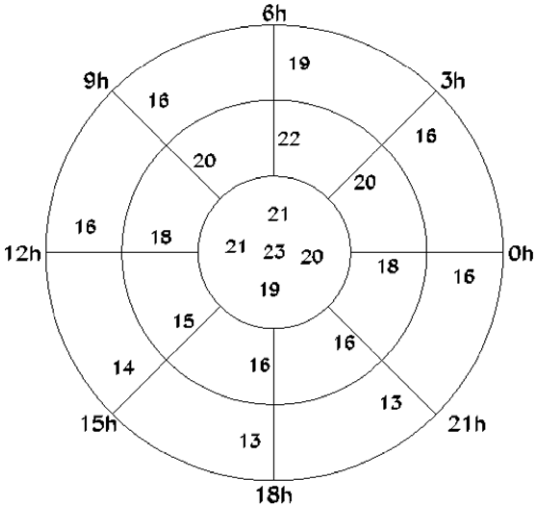

Fig. 15. Numerical values of $N_{.15}$ – the mean number of source events for which signal was declared in 90% or better of 400 trials with a cut on $F = .15$ – at 21 grid points in the Northern Hemisphere. Exact numbers and locations of gridpoints are given in Table 1. The systematic uncertainty in the calculation of $N_{.15}$, due to uncertainties in the size of the error ellipses, is $\leqslant 1$ event.

7. Discussion

As described in Sections 6.1 and 6.2 of this paper, a search for point-like excesses of hadronic cosmic rays at energies greater than $10^{18.5}$ eV can generally be regarded as a search for point-like sources of neutrons. Protons and heavier charged nuclei could contribute to a point-like excess only if they are accelerated nearby enough and if the intervening magnetic fields are weak enough. We reiterate that the present analysis is insensitive to gamma-induced showers.

In Sections 4 and 6, we pointed out that there are small differences in detector aperture and arrival direction uncertainties for nucleons and heavier nuclei. The reconstruction aperture is somewhat smaller, and the angular uncertainty somewhat larger, for iron-induced showers than for nucleon-induced showers. Therefore, in determining the sensitivities and upper limits in Sections 1, we have chosen to simulate our sources under the more conservative assumption that they have the same mixed composition as the isotropic background. The present limits should be reduced by approximately 15% under the strict neutron-source interpretation.

Throughout this work, we make the assumption that the background is indeed isotropic at this level of sensitivity. This is reasonable, given that despite several reports, there are no confirmed excesses as of this writing. Of course, the inclusion of any such non-isotropic excess would weaken

our sensitivity (by increasing the number of background events), so we include in Table 1 our expected background within a 2.5° circle surrounding the gridpoints. Using this information, the expected impact on our analysis can be readily determined for any hypothetical fluctuations in these background levels.

HiRes does not have exposure to the galactic center, on which most neutron-source models have focused. However, the present analysis excludes point-like sources in the northern hemisphere at a level below SUGAR's reported flux of (2.7 ± 0.9) km^{-2} yr^{-1}, for a point excess located 7.5° from the galactic center.

The historically interesting source candidate in the direction of Cygnus X-3 (RA 20.5 h, DEC 40.7°) is very near the grid point located at RA 20.5 h, DEC 45°. We place a 90% c.l. flux upper limit from a point-like source in the vicinity of Cygnus X-3 at 0.5 hadronic cosmic rays above $10^{18.5}$ eV per km^2 yr. Previous Cygnus X-3 flux results were drawn from events samples with energies above 5×10^{17} eV, so a direct comparison is impossible. We can infer – assuming that any cosmic rays from Cygnus X-3 have an energy spectrum similar to that of the full sky – that an extrapolation of our result is not competitive with prior upper limits for events above 5×10^{17} eV. However, this is the first point-like excess search for a high-statistics sample above $10^{18.5}$ eV.

In conclusion, we have conducted a search for point-like excesses in the arrival direction of ultra-high energy cosmic rays with energy exceeding $10^{18.5}$ eV in the northern hemisphere. We place an upper limit of 0.8 hadronic cosmic rays/(km^2 yr) (90% c.l.) on the flux from such excesses across the entire sky and place more stringent limits as a function of position. The HiRes-I monocular data is thus consistent with the null hypothesis for point-like sources of hadronic cosmic rays in this energy range.

Acknowledgements

This work is supported by US National Science Foundation Grants PHY-9321949 PHY-9974537, PHY-9904048, PHYS-0636162, PHY-0140688, and by the Department of Energy Grant FG03-92ER40732. M.A.K. acknowledges the support of a Montana Space Grant Consortium Fellowship. We gratefully acknowledge the contributions from the technical staffs of our home institutions and the Utah Center for High Performance Computing. The cooperation of Colonels E. Fischer and G. Harter, the US Army, and the Dugway Proving Ground staff is greatly appreciated.

References

[1] N. Hayashida et al., Astropart. Phys. 10 (1999) 303.
[2] J.A. Bellido, R.W. Clay, B.R. Dawson, M. Johnston-Hollitt, Astropart. Phys. 15 (2001) 167.
[3] G.L. Cassiday et al., Phys. Rev. Lett. 62 (1989) 383.
[4] M. Teshima et al., Phys. Rev. Lett. 64 (1990) 1628.
[5] M.A. Lawrence et al., Phys. Rev. Lett. 63 (1989) 1121.
[6] A. Borione et al., Phys. Rev. D55 (1997) 1714.
[7] T. Doi et al., in: Proceedings of 24th ICRC, Rome, 2, 1995, p. 804.
[8] R.U. Abbasi et al., Astrophys. J. 623 (2005) 164.
[9] R.U. Abbasi et al., Astropart. Phys. 22 (2004) 139.
[10] R.U. Abbasi et al., Astrophys. J. 610 (2004) L73.
[11] N. Hayashida et al., Phys. Rev. Lett. 77 (1996) 1000.
[12] M. Takeda, et al., in: Proceedings of 27th ICRC, Hamburg, 2001, p. 345.
[13] M. Teshima, et al., Proceedings of 28th ICRC, Tsukuba, 2003, p. 437.
[14] M. Takeda et al., Astrophys. J. 522 (1999) 225.
[15] P.G. Tinyakov, I.I. Tkachev, JETP 74 (2001) 445;
P.G. Tinyakov, I.I. Tkachev, Astropart. Phys. 18 (2002) 165.
[16] D.S. Gorbunov et al., Astrophys. J. 577 (2002) L93.
[17] M.P. Véron-Cetty, P. Véron, ESO Scientific Report, 2000;
M.P. Véron-Cetty, P. Véron, Astron. Astrophys. 374 (2001) 92.
[18] R.U. Abbasi et al., Astrophys. J. 636 (2006) 680.
[19] D.S. Gorbunov, P.G. Tinyakov, I.I. Tkachev, S.V. Troitsky, JETP Lett. 80 (2004) 145.
[20] L.M. Widrow, Rev. Mod. Phys. 74 (2003) 775.
[21] G.R. Farrar. astro-ph/0501388.
[22] G.R. Farrar, A.A. Berlind, D.W. Hogg, Astrophys. J. 642 (2006) L89.
[23] G.A Medina-Tanco, A.A. Watson, in: Proceedings of the 27th ICRC, Hamburg 531, 2001.
[24] M. Bossa, S. Mollerach, E. Roulet, J. Phys. G: Nucl. Part. Phys. 29 (2003) 1409.
[25] P.L. Biermann, G.A. Medina-Tanco, R. Engel, G. Pugliese, Astrophys. J. 604 (2004) L29.
[26] R.M. Crocker et al., Astrophys. J. 604 (2005) 273.
[27] F. Aharonian, A. Neronov, Astrophys. J. 619 (2005) 306.
[28] D. Grasso, L. Maccione, Astropart. Phys. 24 (2005) 273.
[29] T. Abu-Zayyad, Ph.D. Thesis, University of Utah, 2000.
[30] G.C. Archbold, Ph.D. Thesis, University of Utah, 2001.
[31] K. Reil, Ph.D. Thesis, University of Utah, 2001.
[32] R.U. Abbasi et al., Phys. Rev. Lett. 92 (2004) 151101.
[33] T. Abu-Zayyad et al., Astropart. Phys. 23 (2005) 157.
[34] B. Stokes, Ph.D. Thesis, University of Utah, 2006.
[35] D.J. Bird et al., Phys. Rev. Lett. 71 (1993) 3401.
[36] D.J. Bird et al., Astrophys. J. 424 (1994) 491.
[37] R. Abbasi et al., Astropart. Phys. 21 (2004) 111.
[38] G.J. Feldman, R.D. Cousins, Phys. Rev. D 57 (7) (1998) 3873.